
Bidirectional Information Flow (BIF) - A Sample Efficient Hierarchical Gaussian Process for Bayesian Optimization

Juan David Guerra^{1,3,*}, Thomas Garbay^{1,3}, Guillaume Lajoie^{2,3}, and Marco Bonizzato^{1,2,3}

¹Polytechnique Montréal, Montréal, Canada

²Université de Montréal, Montréal, Canada

³Mila - Québec AI Institute, Montréal, Canada

{juan.guerra, guillaume.lajoie, marco.bonizzato}@mila.quebec,
thomas.garbay@polymtl.ca

Abstract

Hierarchical Gaussian Process (H-GP) models divide problems into different sub-tasks, allowing for different models to address each part, making them well-suited for problems with inherent hierarchical structure. However, typical H-GP models do not fully take advantage of this structure, only sending information up or down the hierarchy. This one-way coupling limits sample efficiency and slows convergence. We propose Bidirectional Information Flow (BIF), an efficient H-GP framework that establishes bidirectional information exchange between parent and child models in H-GPs for online training. BIF retains the modular structure of hierarchical models — the parent combines subtask knowledge from children GPs — while introducing top-down feedback to continually refine children models during online learning. This mutual exchange improves sample efficiency, enables robust training, and allows modular reuse of learned subtask models. BIF outperforms conventional H-GP Bayesian Optimization methods, achieving up to 85% and 5x higher R^2 scores for the parent and children respectively, on synthetic and real-world neurostimulation optimization tasks.

1 Introduction

Many real-world tasks require optimizing complex, structured parameter spaces under limited data and high-stakes constraints, by iterative trial-and-error. In team sports, success is not just the sum of individual optimal decisions, but emerges from the coordinated interplay between players. In aerospace engineering, Integrated Flight and Engine Control joins the flight control system (wing flaps, rudder, etc.) with the engine control system (throttle, fuel flow) for optimal performance [Smith et al., 1991]. In neuroscientific engineering, designing multi-electrode neurostimulation protocols for a neural interface is costly and data-scarce [Bonizzato et al., 2023]. Bayesian optimization (BO) provides a principled approach to such problems by using a surrogate model to guide the search for optimal parameters. Gaussian Processes (GPs), commonly used as BO surrogates, capture complex functions and uncertainty from small datasets, making them well-suited for these scenarios. However, when the parameter space has an inherent hierarchical structure, modeling it with a single GP can be inefficient. Hierarchical GP models address this limitation by decomposing the task: multiple *child* GPs model different subcomponents of the original problem, and a *parent* GP combines their outputs to drive the overall optimization procedure. This divide-and-conquer strategy leverages the problem’s

*Corresponding Author

structure and has shown promise in practice — for instance, it has been used to tune spatiotemporal neurostimulation parameters for treating neurological disorders [Laferrière et al., 2020], classification of glaucoma through medical images [An et al., 2021], drug development in the pharmaceutical industry [Ruberg et al., 2023], and many more [Hensman et al., 2013, Fyshe et al., 2012, Fox et al., 2007]. Nevertheless, existing hierarchical GP frameworks suffer a key limitation: information flows only upward from children to parent [Lawrence and Moore, 2007, Fyshe et al., 2012, Laferrière et al., 2020]. The parent model treats child predictions as inputs or priors but has no mechanism to adjust or inform the child models in return. This one-way information flow means valuable insights at the parent level (such as interactions between sub-tasks) cannot propagate back down, leading to suboptimal sample efficiency and slow convergence.

In this work, we introduce Bidirectional Information Flow (BIF)², a novel hierarchical GP framework that establishes two-way communication between parent and child models. BIF retains the modularity of the hierarchical approach — each child GP learns its individual subtask — while also incorporating top-down feedback from the parent to refine the children in an online learning process. By allowing the parent and children to continually inform each other, BIF reduces the number of experiments needed and improves the learning robustness. We claim that our Bidirectional Information Flow model is able to 1) improve performance efficiency compared to baseline models, 2) accurately train child models in the hierarchy using sub-responses entirely inferred from the parent model’s environment interaction, following a short initialization period and 3) boost performance of new combination problems with transfer learning of child modules. We show that BIF yields superior performance on both synthetic benchmarks and a real-world neurostimulation protocol design, achieving higher sample efficiency and more reliable learning than conventional unidirectional hierarchical methods. The remainder of this paper details the BIF methodology and its integration into Bayesian optimization, followed by experiments evaluating its performance.

2 Related Work

Hierarchical implementations can be seen across many domains such as disease detection, drug design, neural stimulation, and many more due to the ability of hierarchical models to effectively break down complex tasks into easier to accomplish subtasks [An et al., 2021, Ruberg et al., 2023, Laferrière et al., 2020, Hensman et al., 2013]. Not only do these models have the benefit of being more interpretable, seeing as it is easier to understand a step by step guide compared to a very low level explanation, they also tend to be sample efficient as models approximate state spaces using previously learned subtasks. We aim to take advantage of this structure and adapt it to use Gaussian Processes.

Early hierarchical approaches, like the Hierarchical GP-LVM [Lawrence and Moore, 2007], and subsequent Deep Gaussian Processes [Damianou and Lawrence, 2013], utilize layered GP architectures for capturing intricate, multi-scale patterns from limited data. Multi-task GPs [Bonilla et al., 2007] further exploit correlations across related tasks, enhancing data efficiency through shared covariance structures. Similarly, Fyshe et al. [2012] use low dimensional latent processes to classify magnetoencephalography (MEG) brain recordings of human subjects observing different words. Explicit hierarchical GP-BO methods directly address structured optimization problems. Laferrière et al. [2020] developed hierarchical GP-BO specifically for neurostimulation protocols, demonstrating improved sample efficiency and performance compared to traditional BO by modeling individual stimulation channels as child GPs feeding into a parent GP as a prior to the mean for the combined neurostimulation task. Other work in the field of hierarchical GP-BO was explored by [Hensman et al., 2013] in the field of genomics. However, previous hierarchical GP frameworks predominantly adopt a one-way flow of information [Lawrence and Moore, 2007, Laferrière et al., 2020, Fyshe et al., 2012, Fox et al., 2007]. This limitation restricts adaptability and sample efficiency since parent-level insights cannot refine or inform the child models iteratively. Our proposed Bidirectional Information Flow (BIF) addresses this gap by introducing two-way interactions within the hierarchical GP framework, significantly enhancing both efficiency and adaptability.

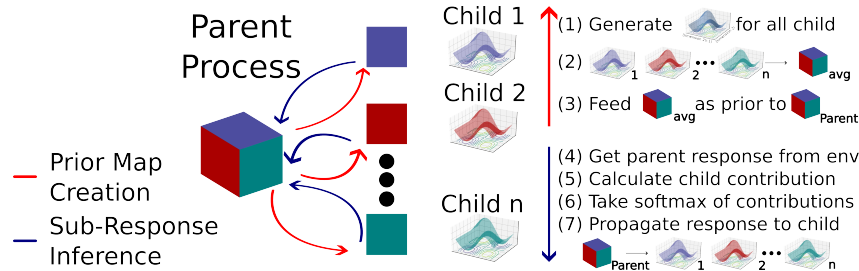


Figure 1: Overview of the BIF framework with an arbitrary number of children. Colour coding demonstrates each child’s responsibility for a parent dimension. Arrows indicate the direction of information flow: red for prior map creation (child to parent, Section 3.2), and blue for sub-response inference via the contribution system (parent to child, Section 3.3). Steps (1–7) summarize Alg. 1.

3 Methodology

We now present our novel algorithm - Bidirectional Information Flow (BIF). We implement a two layer hierarchical structure, wherein the first layer contains a singular parent Gaussian Process (GP) and the second layer consists of n different child GPs learning independent tasks. GPs provide the prediction $p(f(x)|x_n, D_n)$ for a point x where $f(x) \sim GP(\mu(x), k(x, x'))$ with $\mu(x)$ being the mean of the GP for point x and $k(x, x')$ being the covariance function. Background information on GPs and Bayesian Optimization (BO) can be found in Appendix A. The parent learns how to combine the outputs of the children in order to solve a complex goal made of interactions between the children’s tasks. We present this structure in Figure 1. We implement a variety of new techniques to optimize the hierarchical structure of our BIF model: prior map integration for upwards flow of information, a credit contribution system for downwards information flow, and an adaptive data rescaling method.

3.1 Query Selection using Acquisition Maps

For BO to work, we must know what point in the state space to query next for optimization. To do this, we use an acquisition function which leverages the surrogate model to determine the next query location. This generates an acquisition map, where each option in the parameter space is assigned a value relative to how much information may be gained if it were to be selected for querying. In our experiments, BO uses the Upper Confidence Bound (Def. B.1) as its acquisition function due to its optimality as proven in Auer et al. [2002]. An in-depth description of UCB is provided in Appendix B.

Query selection based on prior information is the basis for Bayesian Optimization and guides the decision agent to find optima in the environment. Once the acquisition map has been generated using equation 4 (see Appendix B), the next query location is extracted by finding the maximum value in the map.

3.2 Upwards Information Flow - Prior Maps

In order to efficiently optimize the complex combination task presented to the parent, the parent is given information from the children. The information consists of a state space prediction map from all the children. The children create an acquisition map using UCB, as detailed in Definition B.1, over the entire state space. These acquisition maps are an averaged projection from all the children and is sent to the parent as a prior to the mean. With this information, the parent GP is able to build a rough expectation of the state space to guide its learning.

3.3 Downwards Information Flow - Response Contribution

We present in this section a novel concept based on credit assignment for signal decoupling. To send information downwards from the parent to the children, we develop a contribution system. More

²Code and datasets: refer to our Github at <https://anonymous.4open.science/r/BIF-D04F>

clearly, given an environment response for the combined signal, the children will all take a percentage contribution for that datapoint based on their own predictions on the signal they expect to see for their individual optimization functions. In doing so, we develop a two step process defined mathematically in Definition 3.1.

Definition 3.1. Response Contribution

We define the contribution of child $s \in S$, with S being the set of children, to be as follows:

$$c_s(x) = \frac{\mu_s(x) + \gamma * \frac{\sigma_s(x)}{\sqrt{n_s(x)}}}{\max_{\hat{x}} \left(\mu_s(\hat{x}) + \gamma * \frac{\sigma_s(\hat{x})}{\sqrt{n_s(\hat{x})}} \right)} \quad (1)$$

where $\mu_s(x)$ is the mean, $\sigma_s(x)$ is the uncertainty, as calculated by the child GP, n_s is the query counter for child s at point x , and γ is an uncertainty hyperparameter. We take the contribution of child s for that point to be a fraction over the maximum value of its acquisition function. We can then define a probability distribution using the softmax function to assign credit for the data point:

$$y_s(x) = y_p(x) * \frac{e^{c_s(x)}}{\sum_j^S e^{c_j(x)}} \quad (2)$$

Where y_p represents the environment response for the parent’s combined response. We have then created a probability distribution that, when multiplied with the parent response, gives an expected decomposed value for the children.

Using the contribution system, we can create approximate data points for the children based on information received through the parent. In essence, the contribution system creates a simulated environment for the children, making each parent data point trickle-down information to the children, even if the latter are not directly querying the real environment. These data points can then be added to the children’s training set, allowing for a highly efficient pipeline. This system is how information is sent from the parent to the children.

3.4 Adaptive Data Rescaling

As was introduced in Section 3.3, the training data for BIF comes from two streams, the original initialization set coming from the true environment and the downwards information flow set coming from the response contribution approximation. Drawing datapoints from, what is in essence two different distributions, requires ensuring that the child models are able to draw the correct information from both datasets. To achieve this, we use an adaptive rescaling method where data points are shifted and scaled to be in the range [0, 1], where the lowest valued datapoint is set to 0, the highest set to 1, and the rest maintain their relative position. Let us define a dataset $D_n = \{x_i, y_i\}_{i=0}^n$ and a transformation function $T : Y \rightarrow Z$ such that $T(y_i) = \frac{y_i - \min(Y)}{\max(Y) - \min(Y)}$. Then we can define the normalized dataset $\hat{D}_n = \{x_i, T(y_i)\}_{i=0}^n$ where $x_i, y_i \in D$ for all $i < n$. Now, with this concept we can rescale the two datastreams in parallel where the true data has its normalization function T and the approximated data a separate transformation function T' .

3.5 Training Bidirectional Information Flow

With all necessary modules defined, we can now present the training pipeline for BIF. To begin the training, we need to define a starting dataset of arbitrary size for the child GP models. This is due to the children requiring rudimentary knowledge of the state space to start predicting contributions. The parent model also benefits from this compositional advantage. Then, we initialize the children models and add the starting dataset to their training points. From here, we loop over the training setup involving parent prior map creation, query selection, response contributions propagated to children, and learning outlined in Algorithm 1. Note that in the algorithm, the maximum query budget Q is arbitrary and can be left as a continual learning setup until either a budget, runtime, or desired performance is reached. This paper uses a maximum query budget as the stopping criteria for training.

Algorithm 1 Bidirectional Information Flow

- 1: Initialize model datasets with r datapoints for all child and parent models
 - 2: **for** q in Q **do** ▷ Q is the maximum query budget
 - 3: Generate prior map $p_s = \mu_s + \gamma \frac{\sigma_s}{\sqrt{n_s}} \forall s \in S$ ▷ S is the set of children. Section 3.2
 - 4: Create average prior $p_{avg} = \frac{1}{|S|} \sum_s p_s$ ▷ Refer to Section 3.2
 - 5: Pass p_{avg} as prior to the mean for Parent h ▷ Refer to Section 3.2
 - 6: Generate Acquisition Map for Parent $a_h = \mu_h + \kappa \frac{\sigma_h}{\sqrt{n_h}}$ ▷ Refer to Section 3.1
 - 7: Select $x_q = \max_x(a_h(x))$ to be the next query (number q) for parent h
 - 8: Query environment to get $y_h(x_q)$ as the true environment response
 - 9: Calculate contributions $c_s(x_q) = \mu_s(x_q) + \kappa \frac{\sigma_s(x_q)}{\sqrt{n_s(x_q)}} \forall s \in S$ ▷ Refer to Section 3.3
 - 10: Partition parent response to children $y_s(x_q) = y_h(x_q) * \frac{e^{c_s(x_q)}}{\sum_j e^{c_j(x_q)}}$
 - 11: Add respective $x_q, T[y(x_q)]$ to each GP’s training set ▷ Refer to Section 3.4
 - 12: Increment appropriate query counter for each model in hierarchy
 - 13: Run training for t steps for all models on respective new datasets
 - 14: **end for**
-

4 Experiments

4.1 Implementation Details

As can be seen in Algorithm 1, there are a few hyperparameters that must be set for the model to run such as κ, γ, r , and, t as well as a few additional hyperparameters inherent to GPBO. We run an independent hyperparameter study to determine the optimal hyperparameters for each application and model. These experiments are presented in the Appendix C. Analyzing the hyperparameter studies, we determine that, in general, the optimal hyperparameters for the BIF pipeline are as follows: $\kappa = 9.5, \gamma = 3, r = 6$, and $t = 10$ for synthetic datasets and $\kappa = 4.0, \gamma = 3, r = 6$, and $t = 10$ for the neurostimulation. For the child GPs, we use a Matern Kernel with a lengthscale parameter set to $\nu = 0.5$ while the parent uses an additive kernel where the kernels for each children are summed $kernel_p = \sum_s kernel_s$. For the parameter updates, the ADAM optimizer is used with a learning rate of $\alpha = 0.01$ for both the parent and child GP models. The models were run without the use of GPU acceleration and implemented using the GPyTorch Library [Gardner et al., 2021]. Approximate runtime is 1.5 query/s with a maximum budget of 100 queries on Intel 12th Gen i7 processor with 32 Gb of memory.

4.2 Datasets

Evaluation of the BIF model is done on optimization of three key datasets, each highlighting a different aspect of the model’s performance. The first dataset is a two-dimensional synthetic dataset, where data is generated via a hierarchical process itself: from two children in the hierarchy and one parent. Data is generated through arbitrary functions with a combination in the parent as follows: $f(x) = \frac{\sin(2\pi x)}{x-1} + 2, g(y) = \frac{\sin(2\pi y)}{y-2} + 2$, and parent function $h(x, y) = \frac{f(x)+g(y)}{(x-y)^2+\epsilon}$. In this case, the two children GPs aim to optimize functions f, g and feed their knowledge as a prior to the parent. The parent integrates the priors to boost its performance in optimization function h . The next dataset used in this study is a higher dimensional 3D dataset with three children and one parent. The functions constituting this optimization set are as follows: $f(x) = -(x-2)^5, g(y) = \sin^3(y), k(z) = \frac{\log(z+1)+1}{z+1}$ and parent function $h(x, y, z) = (f(x) + g(y) + k(z))^2 + 2$. The goal of this dataset is to show the robustness of the BIF architecture to learn higher dimensional tasks. Both synthetic datasets have 10% noise added as described in Section 4.5. The final dataset is the optimization of a neurostimulation dataset with two child targets and one parent generated by combining the stimulation of the two children [Laferriere, 2019]. Inputs to the children are the electrode channel on an electrode array implanted in the motor cortex of a non-human primate with the target being maximal muscle activation. This dataset aims to show the applicability of BIF to real-world engineering problems, where success could dictate the implementation of BIF to in-vivo neurostimulation protocols.

4.3 Child Process Modularity

Our model claims to have modular child components that can be reused across tasks. To validate our claim, we present an experimental protocol involving the pretraining of child GPs on one combination task, to later be switched into another combination task. For instance, take two pretraining optimization tasks f with children a, b and g with children c, d . Now we propose an experiment to optimize task h with child targets a, d by inserting the pretrained children from tasks f, g to bootstrap the performance of task h . Further details for this task are provided in Appendix E. As a baseline, a regular BIF model will be trained from scratch to compare the boost in performance seen by injecting the pretrained children to the training protocol.

4.4 Nonlinearity Breaking Point

To elucidate the limitations of our model, we present experiments aimed at targeting the weaknesses of the BIF model. As can be seen in the methodologies section, the composition of the prior maps (Section 3.2) and the contribution system (Section 3.3) assume an intrinsic quasi-linear relationship between the children when being combined to the parent task. With this assumption, we aim to see to which point of nonlinearity can the BIF model still learn efficiently before its inductive biases break down. We propose 3 forms of nonlinearity in order to understand better what domains the model is robust to:

- Exponential Nonlinearity: $h(x, y) = [f(x) + g(y)]^\alpha$
- Exponential Inside Nonlinearity: $h(x, y) = f(x)^\alpha + g(y)$
- Multiplicative Factor Nonlinearity: $h(x, y) = f(x) + g(y) + \alpha f(x)g(y)$

α scales the degree of nonlinearity. We set $f(x) = \sin(x)$ and $g(y) = \tanh(y)$ as simple child objectives to highlight how nonlinearity affects learning via BIF.

4.5 Robustness to Noise

Finally, we investigate the model’s performance compared to baseline models as more noise is introduced to the model. This is implemented by adding a noise scaling factor where at each query to the environment, noise is sampled from a Normal distribution and added to the environment response such that $y_{noisy} = y + \beta * \phi$ where $\phi \sim N(0, \max Y - \min Y)$, Y denotes range of possible outputs, and β is a parameter that adjusts the amount of noise present in the dataset. With this setup, we scale β to see how robust the model is as noise increases.

4.6 Performance Metrics

In all of our analyses, we report the following key metrics: Relative Optimum (RO) of the parent, R^2 coefficient of correlation for the parent – and, when applicable, the R^2 coefficient of correlation of the children. We define the Relative Optimum of the parent to be as follows $RO = \frac{y(\hat{x})}{y(x)}$ such that $\hat{x} = \arg \max \mu(\hat{x}) + \kappa * \frac{\sigma(\hat{x})}{\sqrt{n}}$, x is the ground truth maximum location, y is the true function, and μ, κ and n are the learned parameters of the GP. Relative Optimum then reports the percentage of the maximum reward the model would attain given its prediction of the optimal location relative to the ground truth optimum. The coefficient of correlation, R^2 , is a metric used to evaluate how related two distributions are to each other. We calculate the coefficient of correlation by querying the model at each environment state and recording the predicted response. From this, we compare it to the true space to evaluate how closely the models are able to reconstruct their environments as a whole. This procedure is done for the parent environment and averaged for the children. Both these metrics are on a scale of $[0, 1]$ with 1 being the optimum. Finally, the Global Area Under the Curve (AUC) provides a summary of all these metrics over training, as it calculates the sum of the aforementioned metrics over the training run. This allows us to see in one metric how the performance of the model evolves over training, with higher values indicating earlier training spikes and overall better performance.

Dataset	Model	Relative Optimum	Parent R^2	Child R^2	Global AUC
Synthetic 2D	Vanilla GPBO	83.51	86.37	-	13,383.17
	Laferrière	98.81	92.10	60.70	21,271.38
	BIF	96.40	88.26	87.66	22,611.22
Synthetic 3D	Vanilla GPBO	44.70	41.36	-	5,068.68
	Laferrière	37.67	46.78	8.75	6,000.55
	BIF	68.27	86.34	50.74	13,740.73
Neural Stimulation	Vanilla GPBO	90.84	82.70	-	14,638.65
	Laferrière	98.07	93.81	37.32	18,906.40
	BIF	95.99	96.35	71.72	21,910.59

Table 1: Summary of performance metrics after 100 queries of training. Note that Vanilla GPBO denotes a non-hierarchical GPBO method consequently removing its ability to represent the child R^2 task. Performance metrics are described in Section 4.6

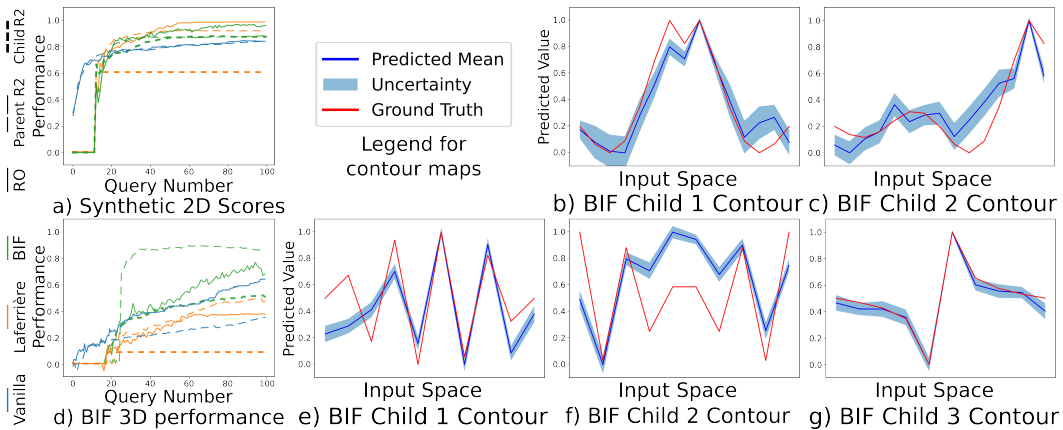


Figure 2: Baseline GPBO models vs. BIF on 2D (a-c) and 3D (d-h) synthetic tasks. (a) shows all model performance for the 2D task; (b-c) show BIF child environment reconstructions (blue: predicted mean/uncertainty, red: ground truth). (d) shows all model performance on the 3D task; (e-g) show BIF child environment reconstructions for 3D, analogous to (b-c). See Section 4.2 for details. Parent Visualizations for 2D available in Appendix D.

5 Results

5.1 Synthetic Two Dimensional Dataset

As a first set of analyses, we run our BIF model on the 2D dataset outlined in 4.2 compared to a baseline vanilla GPBO and an algorithm based on Laferrière et al. [2020] on the same dataset with results reported in Table 1 and Figure 2 (a-c). Both Laferrière and BIF models require an initialization period for the children as detailed in Section 4.1 and transfer the information from the children to the parent. Since the Global AUC sums over all query points, quicker learning will result in a higher Global AUC which we see in both hierarchical models. Evidently, the information provided by the children is substantial, allowing the parent model to quickly outperform the vanilla GPBO in the relative optimum score, parent R^2 , and Global AUC of Synthetic 2D in Table 1. We can see both Laferrière et al. [2020] and BIF exhibit similar learning trajectories for the parent models, demonstrating that the changing parameters for the child while learning do not significantly affect the parent’s performance. In contrast to the parent, we see the largest margin of difference with respect to performance when looking at the coefficient of correlation for the children in the finely dotted lines of Figure 2(a). Due to the definition of the baseline Laferrière model, the children do not learn past their initialization sets, freezing their R^2 score. Observing the training dynamics of the BIF model’s children, we see substantial gains in performance following the random initialization set, where the only information being received is through the contribution method outlined in Section 3.3. These gains in performance highlight the contributions of our work, allowing parallel training

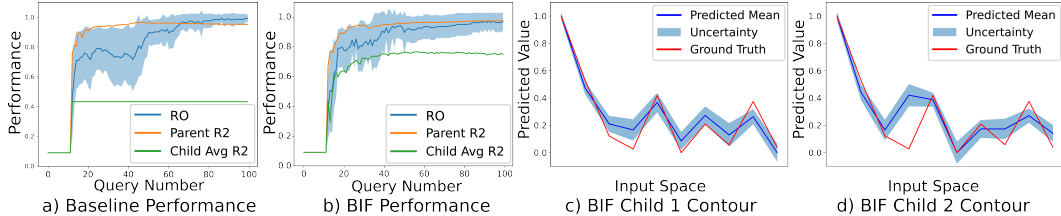


Figure 3: Baseline Laferrière et al. [2020] (a) vs. BIF (b–d) on a real-world neurostimulation task, averaged over 30 runs. (a-b) show overall performance metrics, with BIF achieving higher parent and child R^2 but lower relative optimum. (c-d) show example BIF child belief contours (blue: prediction; red: ground truth). Parent Visualizations available in Appendix D.

of the hierarchy with only one information source. A more in depth interpretation of this difference is visualized in Figure 2 (c-d) where the children’s belief space (blue line) is plotted against the ground truth (red line). We can see the model’s child R^2 score of 87.66 is sufficient for modeling the environment and accurately discovering the maximum location.

5.2 Synthetic Three Dimensional Dataset

The three dimensional dataset is where we see the largest performance boost with BIF compared to the two baselines seen in Table 1. As a summary measurement, we refer to the Global AUC metric. In this column of Table 1, we demonstrate that BIF is able to improve the performance of both the other models by over 100%. A near doubling in performance is also seen in both the coefficients of correlation for the parent and children, where the parent R^2 is 85% higher than the Laferrière model and the child R^2 improving over fivefold. The RO score is where we see the smallest advantage in performance, with vanilla GPBO ranking second for this metric and being outperformed by 53%. The drastic increases in performance here is an indicator of BIF’s ability to handle complex datasets, far superior than previous baseline models. These metrics for BIF are further described in Figure 2, where the training trajectories are shown. Here we demonstrate the efficiency of our model, with all performance metrics achieving nearly their full performance by 50 queries on a task with 10 times more states than the two dimensional task of Section 5.1. We also emphasize the efficacy of the upwards and downwards information flow outlined in Sections 3.2 and 3.3 as the learning of the children and parent begin much lower than in the two dimensional setting but are still able to extract meaningful information from the environment to train the children. These observations verify the claim of the efficiency of our novel method as well as the efficacy of the contribution system in training the children on a mostly inferred training dataset.

5.3 Neurostimulation Dataset

As introduced in Section 4.2, all models were tested on a real-world environment of neurostimulation optimization [Laferrière, 2019]. The results of this testing are presented in row 3 of Table 1 and Figure 3. Both Laferrière et al. [2020] and BIF outperform Vanilla GPBO in all metrics with BIF achieving the highest R^2 scores for both parent and child. Notably, BIF outperforms Vanilla GPBO in the parent R^2 by approximately 14 points and nearly doubles the average child R^2 of the Laferrière model. These results are visualized in Figure 3 (a-b) as the training curves of Laferrière et al. [2020] and BIF respectively. It is clear that the contribution system presented in Section 3.3 is highly effective, quickly improving the average coefficient of correlation for the children. For a more detailed representation of this metric, Figures 3 (c-d) depict an example child GP representation of the state space following the training protocol. Although the average child R^2 reaches only 71.72%, the visualization of the predicted vs true environment state spaces shows that the models are accurately depicting the responses of the neurostimulation set as was also seen in the child contours of Figure 2. With these results we verify our claim that our Bidirectional Information Flow method is able to accurately reconstruct the environment of real-world environments with a training dataset inferred by the contribution system approximation. Less noticeable than the child performance is the improvement in the parent’s R^2 score, improving the performance of the Laferrière model by more than 3% and ultimately a lesser drop in the RO score of the BIF model. The discrepancy in

these scores could be attributed to the influence of uncertainty in the RO score, while the R^2 only uses the mean predictions of the model. We focus on improving the child R^2 over the RO score due to the novelty of the downward information flow. We prove this tradeoff in scores in Appendix C through the hyperparameter testing of our model showing higher RO scores for lower kappa values and higher child R^2 with higher kappa.

5.4 Modularity Results

One of the many benefits of using hierarchical structures is the segmentation of tasks to different modules. We take advantage of this characteristic with a set of experiments briefly described in Section 4.3 and in more detail in Appendix E. The results of these tests are presented in Figure E. We see an expected change in performance from the modularity, with early performance improved when inserting good information, children pretrained on the correct task, to the hierarchy and reduced performance when using bad information, children pretrained on the incorrect task. However, all modular constructions are eventually surpassed in performance by the baseline BIF model with enough training points. This could be due to information from the wrong optimization task being leaked to children under the same parent. We expect as children are continually swapped to more optimization tasks, this effect will disappear as the underlying GP will be able to effectively remove all the noise with more training. With these results, we not only validate the ability to boost performance by inserting previously trained children to new optimization tasks, but also validate the importance of the upwards information flow method as it is shown that bad information flow from children to the parent impairs the parent’s performance.

5.5 Nonlinearity Effects

We assess BIF’s robustness to nonlinear interactions between subtasks, a key assumption underlying the model (Section 4.4). As illustrated in Figure 7, RO scores remain stable across tests, particularly under multiplicative nonlinearity (Fig. 7c). However, substantial impacts arise in exponential scenarios: the parent’s R^2 decreases by 22% and the child’s R^2 by 28% (Fig. 7a), while the simplified exponential-inside test results in a smaller, 10% reduction in child R^2 (Fig. 7b). These findings demonstrate that BIF sustains robust performance overall, with noticeable performance deterioration limited to strongly nonlinear interactions. Extended analysis is available in Appendix F.

5.6 Robustness to Noise

We further evaluate BIF’s robustness in noisy conditions, essential for real-world applications of any machine learning model. As shown in Figure 8, the parent’s R^2 remains remarkably stable despite increased noise, indicating robust learning of the overarching task (Fig. 8b). In contrast, the RO score and average child R^2 are more affected, decreasing by 19% and 31%, respectively, as noise levels rise from 0.1 to 0.5 (Figs. 8a,c). Nevertheless, the child models consistently exhibit incremental improvement in R^2 (mean gain 0.23, std 0.017), suggesting stable learning despite elevated noise conditions. Additional details can be found in Appendix G.

6 Conclusion

In conclusion, we have presented Bidirectional Information Flow (BIF), a hierarchical GP-based Bayesian Optimization framework that introduces a two-way communication mechanism between parent and child models. By leveraging upward prior map aggregation and a novel downward contribution-based signal decoupling scheme, BIF allows the parent and children GPs to continuously inform each other. This bidirectional interaction retains the modular design and interpretability of hierarchical models while overcoming the one-way information flow limitations of prior approaches.

Empirical results on 2D and 3D synthetic benchmarks and a real-world neurostimulation optimization task demonstrate that BIF significantly improves sample efficiency and overall optimization performance compared to conventional unidirectional hierarchical Bayesian Optimization while effectively disentangling signals for child training. The proposed method achieved faster convergence with fewer trials and maintained high predictive accuracy even in the presence of substantial observation noise and nonlinear inter-task interactions. These strengths position BIF effectively for online learning and costly iterative experiments, such as high-stakes domains neurostimulation optimization as framed

in Laferrière et al. [2020] where BIF can accelerate discovery while maintaining reliability under uncertain conditions.

Despite its advantages, BIF remains computationally intensive, incurring an $O(n^3)$ complexity per Gaussian Process in the hierarchy. Continuous training, especially in modular setups as Section 4.3, leads to high computational costs. This could be addressed with a scheduler for bidirectional updates, letting information flow at regular, specifiable intervals rather than each step. Additionally, BIF requires training separate parent processes for each task combination, risking combinatorial explosion with increasing child targets. Future work could address this by developing a pretrained, general-purpose parent model, reducing online training demands.

References

- Guangzhou An, Masahiro Akiba, Kazuko Omodaka, Toru Nakazawa, and Hideo Yokota. Hierarchical deep learning models using transfer learning for disease detection and classification based on small number of medical images. *Scientific Reports*, 11(1):4250, March 2021. ISSN 2045-2322. doi: 10.1038/s41598-021-83503-7. URL <https://www.nature.com/articles/s41598-021-83503-7>. Publisher: Nature Publishing Group.
- Peter Auer, Nicolò Cesa-Bianchi, and Paul Fischer. Finite-time Analysis of the Multiarmed Bandit Problem. *Machine Learning*, 47(2):235–256, May 2002. ISSN 1573-0565. doi: 10.1023/A:1013689704352. URL <https://doi.org/10.1023/A:1013689704352>.
- Edwin V Bonilla, Kian Chai, and Christopher Williams. Multi-task Gaussian Process Prediction. In *Advances in Neural Information Processing Systems*, volume 20. Curran Associates, Inc., 2007. URL https://papers.nips.cc/paper_files/paper/2007/hash/66368270ffd51418ec58bd793f2d9b1b-Abstract.html.
- Marco Bonizzato, Rose Guay Hottin, Sandrine L. Côté, Elena Massai, Léo Choinière, Uzay Macar, Samuel Laferrière, Parikshat Sirpal, Stephan Quessy, Guillaume Lajoie, Marina Martinez, and Numa Dancause. Autonomous optimization of neuroprosthetic stimulation parameters that drive the motor cortex and spinal cord outputs in rats and monkeys. *Cell Reports Medicine*, 4(4):101008, April 2023. ISSN 2666-3791. doi: 10.1016/j.xcrm.2023.101008. URL <https://www.sciencedirect.com/science/article/pii/S2666379123001180>.
- Andreas Damianou and Neil D. Lawrence. Deep Gaussian Processes. In *Proceedings of the Sixteenth International Conference on Artificial Intelligence and Statistics*, pages 207–215. PMLR, April 2013. URL <https://proceedings.mlr.press/v31/damianou13a.html>. ISSN: 1938-7228.
- Emily B. Fox, Erik B. Sudderth, and Alan S. Willsky. Hierarchical Dirichlet processes for tracking maneuvering targets. In *2007 10th International Conference on Information Fusion*, pages 1–8, July 2007. doi: 10.1109/ICIF.2007.4408155. URL <https://ieeexplore.ieee.org/document/4408155>.
- Alona Fyshe, Emily Fox, David Dunson, and Tom Mitchell. Hierarchical Latent Dictionaries for Models of Brain Activation. In *Proceedings of the Fifteenth International Conference on Artificial Intelligence and Statistics*, pages 409–421. PMLR, March 2012. URL <https://proceedings.mlr.press/v22/fyshe12.html>. ISSN: 1938-7228.
- Jacob R. Gardner, Geoff Pleiss, David Bindel, Kilian Q. Weinberger, and Andrew Gordon Wilson. GPyTorch: Blackbox Matrix-Matrix Gaussian Process Inference with GPU Acceleration, June 2021. URL <http://arxiv.org/abs/1809.11165>. arXiv:1809.11165 [cs].
- James Hensman, Neil D. Lawrence, and Magnus Rattray. Hierarchical Bayesian modelling of gene expression time series across irregularly sampled replicates and clusters. *BMC Bioinformatics*, 14(1):252, August 2013. ISSN 1471-2105. doi: 10.1186/1471-2105-14-252. URL <https://doi.org/10.1186/1471-2105-14-252>.
- Samuel Laferrière. `samlaf/hierarchical-gaussian-process`, July 2019. URL <https://github.com/samlaf/hierarchical-gaussian-process>. original-date: 2019-07-06T19:14:22Z.

- Samuel Laferrière, Marco Bonizzato, Sandrine L. Côté, Numa Dancause, and Guillaume Lajoie. Hierarchical Bayesian Optimization of Spatiotemporal Neurostimulations for Targeted Motor Outputs. *IEEE Transactions on Neural Systems and Rehabilitation Engineering*, 28(6):1452–1460, June 2020. ISSN 1558-0210. doi: 10.1109/TNSRE.2020.2987001. URL https://ieeexplore.ieee.org/abstract/document/9062604?casa_token=3F0As8DHhk0AAAAA:xe_5r0HkQiGtRsrwZ04f_Mz80gL017myA94LkISY6yAfow2QnJrRrYchrXNO-drr98gUDAZKeYo. Conference Name: IEEE Transactions on Neural Systems and Rehabilitation Engineering.
- Neil D. Lawrence and Andrew J. Moore. Hierarchical Gaussian process latent variable models. In *Proceedings of the 24th international conference on Machine learning*, ICML '07, pages 481–488, New York, NY, USA, June 2007. Association for Computing Machinery. ISBN 978-1-59593-793-3. doi: 10.1145/1273496.1273557. URL <https://doi.org/10.1145/1273496.1273557>.
- Carl Edward Rasmussen and Christopher K. I. Williams. *Gaussian Processes for Machine Learning*. URL <https://direct.mit.edu/books/oa-monograph/2320/Gaussian-Processes-for-Machine-Learning>.
- Stephen J. Ruberg, Francois Beckers, Rob Hemmings, Peter Honig, Telba Irony, Lisa LaVange, Grazyna Lieberman, James Mayne, and Richard Moscicki. Application of Bayesian approaches in drug development: starting a virtuous cycle. *Nature Reviews Drug Discovery*, 22(3):235–250, March 2023. ISSN 1474-1784. doi: 10.1038/s41573-023-00638-0. URL <https://www.nature.com/articles/s41573-023-00638-0>. Publisher: Nature Publishing Group.
- R. H. Smith, J. D. Chisholm, and J. F. Stewart. Optimizing aircraft performance with adaptive, integrated flight/propulsion control. *ASME, Transactions, Journal of Engineering for Gas Turbines and Power*, 113, January 1991. URL <https://ntrs.nasa.gov/citations/19910039021>. NTRS Author Affiliations: McDonnell Aircraft Co., NASA Flight Research Center NTRS Report/Patent Number: ASME PAPER 90-GT-252 NTRS Document ID: 19910039021 NTRS Research Center: Legacy CDMS (CDMS).
- Petru Tighineanu, Kathrin Skubch, Paul Baireuther, Attila Reiss, Felix Berkenkamp, and Julia Vinogradska. Transfer Learning with Gaussian Processes for Bayesian Optimization, March 2022. URL <http://arxiv.org/abs/2111.11223>. arXiv:2111.11223 [stat].

A Gaussian Process based Bayesian Optimization

In the search for an efficient machine learning method to solve optimization tasks, few options are able to outperform Gaussian Processes (GP) based Bayesian Optimization (BO) in the low data regime. Bayesian Optimization is an iterative optimization algorithm where surrogate models predict which next query will provide the most information to the model based on the set of previous environment queries. BO provides access to uncertainty predictions on top of the expected reward from the different actions in the space, allowing for the application of these algorithms into high risk scenarios where knowledge of the potential errors in a prediction is paramount. BO aims to optimize an unknown optimization function $f : X \rightarrow \mathbb{R}$ where after each iteration, a new evaluation of the optimization function $y_i = f(x_i)$ is added to the training dataset $D_n = \{x_i, y_i\}_{i=0}^n$.

Calculation of these estimates is performed by the surrogate model, which we select to be Gaussian Processes due to its excellence in low data regimes with Upper Confidence Bounds as the acquisition function (refer to Section 3.1 for further details). GPs provide the prediction $p(f(x)|x_n, D_n)$ where $f(x) \sim GP(\mu(x), k(x, x'))$ with $\mu(x)$ being the mean of the GP for point x and $k(x, x')$ being the covariance function used to calculate how related two points (x, x') are to each other. We select to use the Matern kernel for the covariance function. To predict the next test point using the GP, we can calculate the mean and variance using the learned noise σ_{ik}^2 as follows:

$$\begin{aligned}\mu(x) &= \mathbf{k}_x^T (K + \sigma_{ik}^2 I)^{-1} \mathbf{y} \\ \sigma(x)^2 &= k(x, x) - \mathbf{k}_x^T (K + \sigma_{ik}^2 I)^{-1} \mathbf{k}_x\end{aligned}\tag{3}$$

such that K represents the $n \times n$ covariance matrix and \mathbf{k}_x represent the $1 \times n$ covariance vector within K corresponding to the point x . A thorough guide on Gaussian Processes can be accessed through Rasmussen and Williams.

B Upper Confidence Bounds

In Bayesian Optimization, the acquisition function guides the search for the optimal query location by quantifying the potential value of evaluating each candidate point in the input space. We adopt the *Upper Confidence Bound (UCB)* as our acquisition function due to its principled trade-off between exploration and exploitation, particularly in data-scarce settings.

Definition B.1 (Upper Confidence Bound). *Given a surrogate Gaussian Process model with posterior predictive mean $\mu(x)$, predictive standard deviation $\sigma(x)$, and query count $n(x)$ for input x , the UCB score is computed as:*

$$UCB(x) = \mu(x) + \kappa \cdot \frac{\sigma(x)}{\sqrt{n(x)}} \tag{4}$$

where:

- $\mu(x)$ represents the surrogate model’s current estimate of the objective at location x (exploitation),
- $\sigma(x)$ captures the model’s predictive uncertainty at x (exploration),
- $n(x)$ denotes the number of times location x has been queried,
- $\kappa \in \mathbb{R}^+$ is a tunable hyperparameter controlling the exploration–exploitation balance.

The UCB acquisition function encourages the model to explore uncertain regions (where $\sigma(x)$ is high) early in training, while progressively prioritizing exploitation as information accumulates and $n(x)$ increases. This dynamic makes UCB especially suitable for online learning systems like BIF, where efficient sample usage is critical.

In BIF, UCB maps are generated independently by each child model over its respective subspace. These maps are then aggregated into a prior map for the parent model (Section 3.2) and reused in the downward contribution mechanism (Section 3.3), thereby ensuring consistent acquisition strategies across the entire hierarchy.

C Hyperparameter Testing and Selection

In Figure 4 we show the hyperparameter search for the neural dataset. As can be seen in 4a, the most sensitive hyperparameter is the kappa value, where higher values result in higher R^2 scores for the children with diminishing scores for the exploration score as kappa is scaled. Next, the gamma value search shows that smaller gamma values improve the performance of the children while the initialization set size and number of training iterations have minimal effects on the end model performance of BIF. Initialization set size seems to have no significant effect on the performance metrics. Contrarily, we observe that more training iterations improve the exploration score and parent R^2 at the cost of higher training times. Balancing these hyperparameters, we selected a kappa value of 4.0, gamma of 3, initialization set size of 6, and 10 training iterations. In the Synthetic 2D dataset for BIF (Fig. 4i-j), we see very similar trajectories for on all hyperparameters except the gamma value, where BIF appears to not be sensitive to this parameter in the Synthetic 2D setup while it affects the child R^2 in the neural dataset.

We run hyperparameter searches for the other models with similar results. Figure 4(m-p) shows an example of these other hyperparameter searches for the Laferrière model on the Synthetic 2D dataset from Section 5.1. We observe in these plots that higher kappa values result in better results for the relative optimum. Gamma has little to no effect in the Laferrière model, leading us to set the gamma value equal to the BIF model at 3. Initialization size has the most dramatic performance difference for the child R^2 as expected. However, due to the minimal effect on the other metrics, we set initialization size equal to BIF to show the performance differences. Finally, the number of training iterations has minimal effect, with fine grained differences making 10 the optimal for the AUC metric.

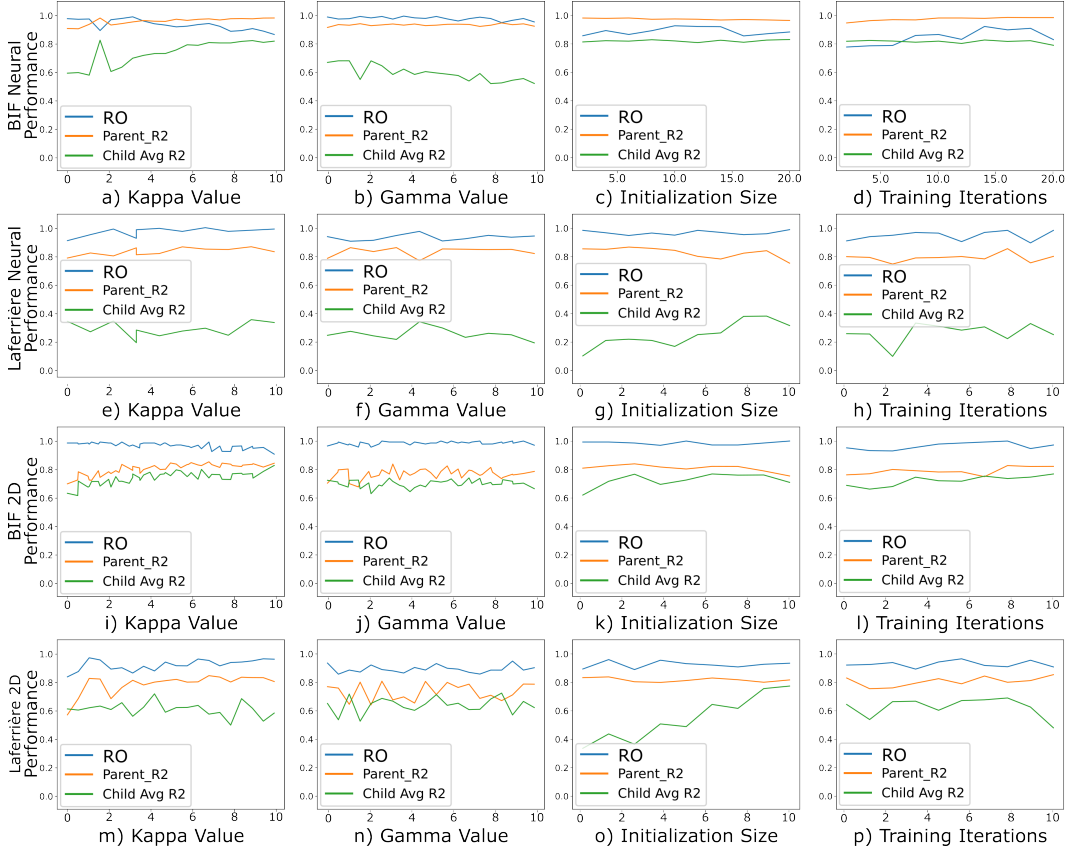


Figure 4: Hyper Parameter Search Results. Due to time constraints and the number of hyperparameters, search is run one by one for each parameter. Baseline parameters are kappa 9.5, gamma 3, initialization set size of 6, and 10 training iterations. (a-d) represent hyperparameter search for BIF and (e-h) for Laferrière on the neural dataset. (i-l) shows the hyperparameter search for BIF and (m-p) for Laferrière on the 2D synthetic dataset.

D Parent Gaussian Process Environment Visualization

In this section, we present the environment reconstruction of the parent processes as done for the children in Figures 2 and 3. Note we cannot display the heatmaps of the Synthetic 3D task from Section 5.2 as this would require a 4D heatmap visualization. Due to this, we strictly rely on the R^2 scores of the parent as a guide for environment reconstruction accuracy. We create these state maps as a way to visualize the R^2 scores presented in the performance figures. All models have the same method applied to them, where they are queried over the entire state space and results are plotted in the 2D heatmap presented in Figure 5. The true heatmap (d,h) represent the ground truth of the environment, setting a baseline of what the other maps should resemble. As reflected in Table 1, the heatmap of BIF has the best reconstruction of the state space for the Synthetic 2D task, with Laferrière et al. [2020] following. Vanilla GPBO is not able to accurately reconstruct this dataset and, consequently, has a much lower R^2 score for the parent. Notably, in this optimization task, BIF is able to find multiple suboptima present in the true heatmap and not found by the other models. For the Neural dataset, we see a similar situation but with Laferrière et al. [2020] leading the models in reconstruction similarity and BIF following closely. Both these models offer accurate reconstructions as can be seen in the heatmaps.

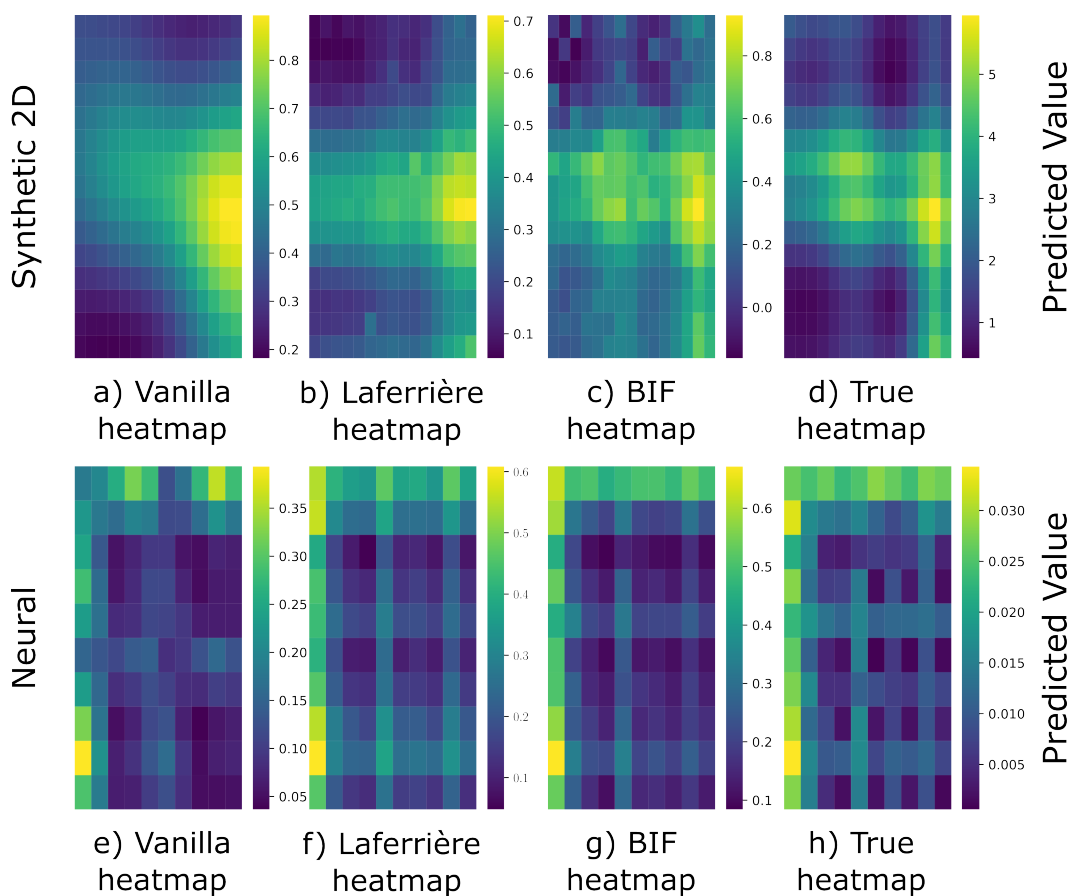


Figure 5: Parent Environment Reconstructions for Synthetic 2D (a-d) from Section 5.1 and Neural Dataset (e-h) from Section 5.3. True heatmap denotes the ground truth and all other heatmaps correspond to a specific model type. The more the heatmaps resemble the ground truth, the higher the R^2 score.

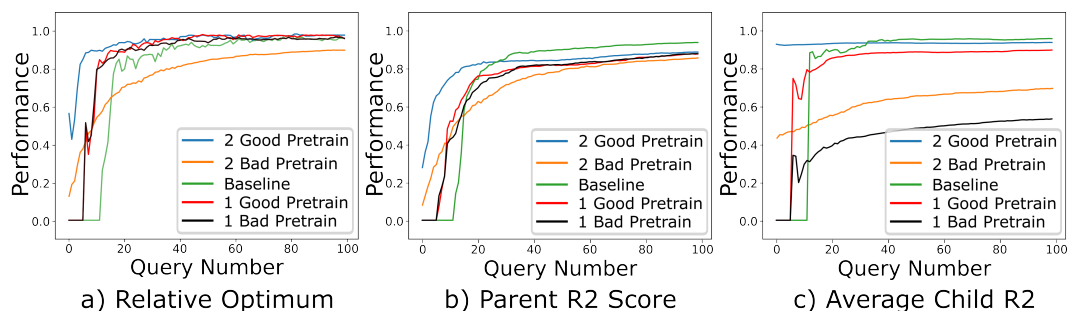


Figure 6: Effect of swapping pretrained children on BIF performance. Good pretraining denotes switching to the same child task and bad denotes using the pretrained child on a different task. Baseline performance is regular BIF training as presented in Algorithm 1.

E Bidirectional Information Flow Modularity

Here we provide a more in depth discussion and interpretation of the modularity experiments. As stated in Section 4.3, these experiments are designed to show one of the key benefits of using a modular structure - the segmentation of tasks. In the BIF setup, we aim to minimize the need of pretraining the children while still providing boosts to the overall optimization goal. In this modularity experiment, the initialization set outlined in the model setup is replaced by inserting children who have been trained previously on a different overarching task. This experiment can be thought of as form of transfer learning, where pretrained modules (i.e. children) are sent to novel tasks to boost performance. Previous works have looked at how hierarchical GPs can efficiently do this type of task [Tighineanu et al., 2022]. We define a set of experiments as the optimization of three different tasks:

1. $f(x) = -(x - 2)^2 + 2$, $g(y) = -\frac{x-1}{2}^4 + 2$, and parent function $h(x, y) = \frac{f(x)+g(y)}{(x-y)^2+\epsilon}$;
2. $f'(x) = \frac{\sin(2\pi x)}{x-1} + 2$, $g'(y) = \frac{\sin(2\pi x)}{x-2} + 2$, and parent function $h'(x, y) = \frac{f(x)+g(y)}{(x-y)^2+\epsilon}$;
3. the modular task $h''(x, y) = \frac{f(x)+g'(y)}{(x-y)^2+2+\epsilon}$

Note that the modular task is made of the child functions from the two previous tasks, allowing the transfer of knowledge between parent optimization tasks. This mimics real-world use of information, where doing a hierarchical task can reuse pretrained information that was previously used to build a different hierarchy.

The "good" children, as shown in Figure 6, have the same underlying optimization function that is input to another parent function while the "bad" children have learned the wrong function and should hinder the performance of the model. With these different types of child transfers, we also add another layer of the number of children transferred, where in a two dimensional task the maximum number of children to transfer is 2, as a hyperparameter to see the sensitivity to the modularity. Each child that must be trained from scratch is given an initialization set of 6 randomly selected points.

We observe in Figure 6 that for early training steps, the pretraining regimen works in boosting the performance of the parent model but is eventually overshadowed by the baseline model. The model shows sensitivity to the number of pretrained children as, with the exception of Figure 6c, having more properly trained children gives better performance while more bad children make the model weaker. We expect the eventual higher performance of the baseline model compared to the properly pretrained models could be due to information from the inserted children containing what can be considered noise from the previous optimization tasks. However, future work could investigate the effect of this noise as the children are continuously swapped into more optimization tasks. This could help the GP find the true function from the noise and we expect a significantly higher performance boost.

F Bidirectional Information Flow Nonlinearity Robustness

Machine learning models are typically constructed with a certain task in mind, leading their architecture to be designed for the given task. In BIF, the target task is neurostimulation optimization, which combines interactions in a predominantly linear manner [Bonizzato et al., 2023, Laferrière et al., 2020]. Here we present the results of the nonlinearity testing outlined in Section 4.4 on BIF to show how the model is able to generalize to child interactions lying outside of its expected domain. Figure 7 illustrates that as α scales, a metric to denote the degree of nonlinearity, the effects are negligible with respect to the relative optimum across all tests, and in the specific case of the multiplicative nonlinearity test, increasing the alpha value has no significant effects on any of the metrics (Fig. 7c). In the two other nonlinearity experiments, Figures 7(a-b), we see a more significant effect on the model. In the exponential experiment (Fig. 7a), the model has a 22% reduction in the parent's R^2 score and a 28% reduction of the average child's R^2 score. In the exponential inside experiment, only the average child R^2 experiences a significant drop of 10% (Fig. 7b), aligning with the fact that it is in essence a simplified version of the exponential experiment. The disproportionate effect of nonlinearity on the children is expected, as the contribution system from which the children train from is the most heavily reliant on the linearity assumption while the other metrics, particularly the parent, is only taking the linearity assumption as a prior to the mean. In light of this, the model is still highly robust to nonlinearity, as only high alpha values are able to affect the model's performance.

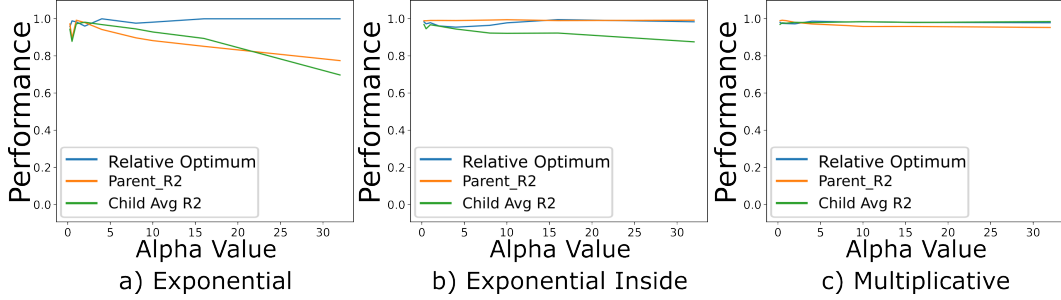


Figure 7: Results of **Nonlinearity Experiments** described in Section 4.4. We aim to show the inherent biases of the model due to the assumption of linear interactions between submodels. Higher α values signify an increase in nonlinearity as shown in the description of the experiments in Section 4.4.

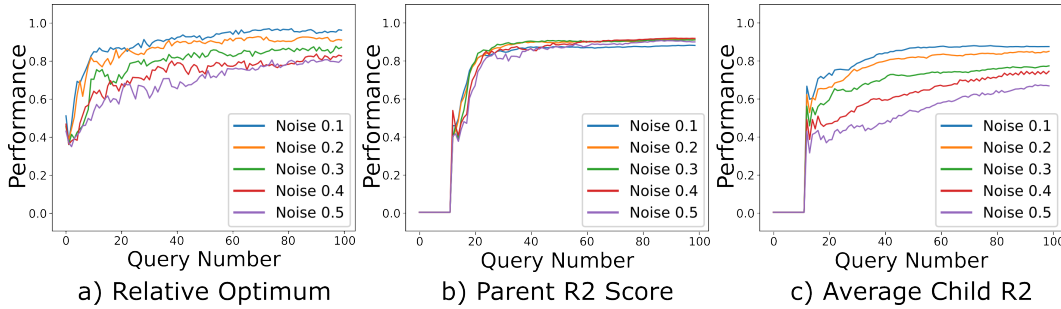


Figure 8: Performance of **Bidirectional Information Flow with Scaling Noise** as detailed in Section 4.5. Higher values of noise mean higher values of β in the description of the experiment in Section 4.5. Relative Optimum is more affected than other metrics with scaling noise, followed by average coefficient of correlation for the children, and parent coefficient of correlation not significantly affected.

G Effects of Noise on Bidirectional Information Flow

Robustness to noise is an important factor when deploying machine learning models to the real world. Typically, a model will be able to learn through the noise when sufficient data points are present. However, in our target application of low data regimes with high noise, such as neurostimulation, our model must be able to deal with this task without the typical solution. In Figure 7, we present the results of scaling noise outlined in Section 4.4. Most notable of the noise testing results is in Figure 8b where the parent R^2 score is seemingly unaffected by the increased noise while the RO score and child R^2 have diminishing scores as noise increases. Interestingly, the child R^2 score looks to have the same amount of information learned as noise increases but with different starting points with higher noise lowering the initial performance. Running a statistical test on this observation shows the average gain in performance is 0.23 points with a standard deviation of 0.017. This suggests that the amount of information learned remains constant with minimal variability as noise is scaled, demonstrating that the BIF model is, in part, robust to noise with respect to the R^2 of the children. Finally, the RO score of the BIF model shown in Figure G is affected most significantly by scaling noise with all instances starting at nearly the same RO score and diverging throughout training with higher noise values resulting in lower RO scores.